Title

Structural dynamics of the ΔE22 (Osaka) familial Alzheimer's disease-linked amyloid β-protein

Journal

Amyloid, 18(3)

ISSN

1350-6129

Authors

Inayathullah, Mohammed
Teplow, David B

Publication Date

2011-09-01

DOI

10.3109/13506129.2011.580399

Peer reviewed

Published in final edited form as:
Amyloid. 2011 September ; 18(3): 98–107. doi:10.3109/13506129.2011.580399.

Structural dynamics of the ΔE22 (Osaka) familial Alzheimer's disease-linked amyloid β-protein

Mohammed Inayathullah[1] and **David B. Teplow, Ph.D.**[1,2,*]

[1]Department of Neurology, David Geffen School of Medicine at UCLA

[2]Molecular Biology Institute and Brain Research Institute, University of California, Los Angeles, California 90095

Abstract

A familial form of Alzheimer disease (AD) recently was described in a kindred in Osaka, Japan. This kindred possesses an amyloid β-protein (Aβ) precursor mutation within the Aβ coding region that results in the deletion of Glu22 (ΔE22). We report here results of studies of [ΔE22]Aβ40 and ΔE22Aβ42 that sought to elucidate the conformational dynamics, oligomerization behavior, fibril formation kinetics, fibril morphology, and fibril stability of these mutant peptides. Both [ΔE22]Aβ peptides had extraordinary β-sheet formation propensities. The [ΔE22]Aβ40 mutant formed β-sheet secondary structure elements ≈400-fold faster. Studies of β-sheet stability in the presence of fluorinated alcohol cosolvents or high pH revealed that the ΔE22 mutation substantially increased stability, producing a rank order of [ΔE22]Aβ42 >> Aβ42 > [ΔE22]Aβ40 > Aβ40. The mutation facilitated formation of oligomers by [ΔE22]Aβ42 (dodecamers and octadecamers) that were not observed with Aβ42. Both Aβ40 and Aβ42 peptides formed nebulous globular and small string-like structures immediately upon solvation from lyophilizates, whereas short protofibrillar and fibrillar structures were evident immediately in the ΔE22 samples. Determination of the critical concentration for fibril formation for the [ΔE22]Aβ peptides showed it to be ≈1/2 that of the wild type homologues, demonstrating that the mutations causes a modest increase in fibril stability. The magnitude of this increase, when considered in the context of the extraordinary increase in β-sheet propensity for the ΔE22 peptides, suggests that the primary biophysical effect of the mutation is to accelerate conformational changes in the peptide monomer that facilitate oligomerization and higher-order assembly.

Keywords

Alzheimer's disease; amyloid®-protein; Osaka mutation; fibril formation; aggregation; oligomerization

INTRODUCTION

Alzheimer disease (AD) is the most common cause of late life dementia [1]. AD is characterized histopathologically by amyloid plaques in the brain parenchyma and vasculature [2]. These plaques are composed predominately of the amyloid β-protein (Aβ) [3], which is present in the human body in two main alloforms, Aβ40 and Aβ42, that differ

[*]**Correspondence:** David B. Teplow, Ph.D. 635 Charles E. Young Drive South (Rm. 445) Los Angeles, CA 90095-7334 Telephone number: 1-310-206-2030 Fax number: 1-310-206-1700 dteplow@ucla.edu.

DECLARATION OF INTERESTS

The authors report no conflicts of interest. The authors alone are responsible for the content and writing of the paper. This work was supported by NIH grant AG027818.

by the presence of an Ile–Ala dipeptide at the C-terminus. Abundant evidence exists supporting the hypothesis that Aβ assembly is the critical pathologic event in AD. Originally, the assembly to which the hypothesis referred was fibril formation [4]. Most recently, Aβ oligomers have been postulated to be the proximate neurotoxins in the disease [5] and a new hypothesis, the "oligomer cascade hypothesis," has been promulgated [6]. However, Aβ assembly is a complex process that produces a large variety of assemblies, most of which are neurotoxic (for a recent review, see [5]). These assemblies range from dimers to larger oligomers and include annuli, spherical structures, and larger protofibrillar species.

Mechanistic insights into Aβ assembly have come from the study of forms of Aβ that are linked to familial AD (FAD). The FAD mutations produce single amino acid substitutions that alter significantly the biophysical behaviors of the resultant peptides. These substitutions, referred to using the ethnicities of the families in which they were identified, include the English (His6Arg) [7], Tottori (Asp7Asn) [8], Flemish (Ala21Gly) [9], Dutch (Glu22Gln) [10, 11], Italian (Glu22Lys) [12], Arctic (Glu22Gly) [13, 14], and Iowa (Asp23Asn) mutations [15]. These mutations produce classical AD, cerebral amyloid angiopathy (CAA), or forms of AD with more pronounced CAA [16, 17]. Recently, a new mutation was discovered that causes the deletion of Glu22 from Aβ (ΔE22) [18]. This "Osaka" mutation was reported to enhance peptide oligomerization but to prevent fibrillization [18].

The discovery of the Osaka mutation was intriguing because of earlier studies that revealed a turn conformation in the Ala21–Ala30 region of Aβ that nucleated monomer folding, thus facilitating higher-order assembly [19]. Importantly, this turn was stabilized by long-range electrostatic interactions between Lys28 and either Glu22 or Asp23. Subsequent studies of the biophysical effects of FAD-linked amino acid substitutions at Glu22 or Asp23 showed that all substitutions altered the stability of the monomer folding nucleus [20]. The Osaka mutation completely eliminates Glu22, thus we hypothesized that a significant effect on peptide assembly should be observed. We tested this hypothesis by chemically synthesizing [ΔE22]Aβ40 and [ΔE22]Aβ42 and then studying the conformational dynamics and assembly of these two peptides. We report and discuss the results of these studies here.

EXPERIMENTAL PROCEDURES

Peptide synthesis

Wild type (WT) Aβ40 and Aβ42, and their ΔE22 analogues, were chemically synthesized, purified, and characterized, essentially as described [21]. Briefly, peptides were synthesized using an automated peptide synthesizer (Model 433A, Applied Biosystems, Foster City, CA) with 9-fluorenylmethoxycarbonyl-based methods. Peptides were purified using reverse phase high-performance liquid chromatography (RP-HPLC). The purity of the peptides was >95%. Quantitative amino acid analysis and mass spectrometry yielded the expected compositions and molecular weights, respectively, for each peptide. Purified peptides were stored as lyophilizates at –20°C.

Sample preparation

All peptides were pretreated with dilute NaOH (5–50 mM) to increase their solubility and decrease *de novo* peptide aggregation [22]. The ΔE22 peptides were found empirically to have very low solubility relative to that of the WT Aβ peptides (see "Discussion" for comments about this important empirical observation). For this reason, the following method was used to prepare these analogues. Peptides were dissolved initially in 50 mM NaOH at a concentration of 1 mg/ml, sonicated for 3 min in an ultrasonic water bath (Model

1510, Branson Ultrasonics Corp., Danbury, CT), and then either were centrifuged at 16000 × *g* for 10 min at 4°C or were filtered with a previously washed (using 50 mM NaOH) 0.02 μm (Anotop™ 10, Whatman) syringe filter. The supernate or filtrate was placed on ice during the initial sample preparation process before neutralizing the solution. The concentrations of the ΔE22 peptides were determined initially by measuring their UV absorbance (ε_{280} = 1480 M^{-1} cm^{-1}). WT Aβ peptides were diluted to produce concentrations equal to those of their ΔE22 analogues (i.e., [Aβ40] = [[ΔE22]Aβ40] and [Aβ42] = [[ΔE22]Aβ42]). An aliquot of the filtrate (10% of the required final volume is defined as 1 v) was diluted with 4 v of water, after which 5 v of 20 mM sodium phosphate buffer, pH 7.4, containing 0.02% (w/v) sodium azide, was added. The pH then was checked using an ORION (model 420A) pH meter and, if necessary, a few μl of 0.5 M HCl was used to adjust the pH to 7.4. Aβ concentrations also were determined *a posteriori* using quantitative amino acid analysis, as described [23]. The final concentrations of the Aβ40 and Aβ42 peptides were 11–13 μM and 6–8 μM, respectively, unless otherwise specified.

Circular dichroism spectroscopy (CD)

Aβ peptides were prepared by centrifugation, as described in *Sample Preparation*. Spectra were acquired periodically during incubation of the peptides at 37°C without agitation. The peptide solution was placed into a 0.1 cm path length quartz cell (Hellma, Forest Hills, NY). Spectra were acquired using a Jasco Model J-810 spectropolarimeter (Jasco, Japan) from ≈190–260 nm at 0.2 nm resolution with a scan rate of 100 nm/min. Ten scans were acquired and averaged for each sample. Raw data were manipulated by smoothing and subtraction of buffer spectra according to the manufacturer's instructions. For some samples, high photomultiplier voltage at low wavelength precluded data acquisition to wavelengths as low as 190 nm. Four independent experiments were performed with each peptide. To determine the midpoint of transitions from starting statistical coil structure to final β-sheet structure, the inflection points of the curves of Θ_{218} versus time at the beginning and end of the steep decline in this metric were determined by visual inspection. The midpoint of the line connecting these two points was considered the midpoint of the transition.

Cosolvent and solvent studies

Peptides were prepared by filtration, as described in *Sample Preparation*. A 20 μl aliquot of the filtrate was diluted with 180 μl of an appropriate mixture of 10 mM sodium phosphate, pH 7.4, and 2,2,2-trifluoroethanol (TFE) or 1,1,1,3,3,3-hexafluoro-2-propanol (HFIP), and then the pH was adjusted to 7.4 by addition of 2 μl of 0.5 M HCl. This procedure produced a final NaCl concentration of 5 mM. Experiments also were performed by solvating lyophilizates directly into the cosolvent. CD spectra were recorded immediately after sample preparation. Four independent experiments were performed.

Fibril nucleation and growth

To study the nucleation activity of [ΔE22]Aβ40, 1 v of this peptide was mixed with 9 v of WT Aβ40, each at a concentration of 12 μM. Similarly, 1 v of [ΔE22]Aβ42 was mixed with 9 v of WT Aβ42. Control reactions were done by simply preparing 10 v of Aβ40 or Aβ42. Each peptide or peptide mixture then was incubated at 37°C without agitation. Fibril assembly was monitored by ThT fluorescence. To do so, a 10 μl aliquot of each reaction mixture was removed periodically and then was mixed with 250 μl of 50 μM ThT in 10 mM sodium phosphate, pH 7.4. Fluorescence intensity was recorded four times at 10 seconds interval and then these intensities were averaged. All samples were blank-corrected. Fluorescence was measured using an Hitachi F4500 fluorometer (Hitachi Instruments Inc., Rye, NH) in which the excitation wavelength was 450 nm (slit width was 5 nm) and the emission wavelength was 480 nm (slit width was 10 nm). Four independent experiments were performed for each sample.

Determination of critical concentration (C_r)

After the ThT fluorescence reached a plateau value, an aliquot of each reaction mixture was centrifuged at 436,000 × *g* for 1 h (TLA100 rotor; 100,000 rpm; Beckman Optima TLX Ultra centrifuge). The concentration of Aβ present in the supernate was quantified by amino acid analysis (AAA). This concentration is equal to the critical concentration, C_r, which is the inverse of the amyloid fibril growth equilibrium constant, i.e., $k = 1/C_r$ [24, 25]. Using this relationship, we calculate ΔG^0, representing the free energy change in the Aβ⇌ fibril equilibrium, according to the equation $\Delta G^0 = -RT \ln (1/C_r)$. Statistical analysis was performed using *t*-tests (paired) and Mann Whitney Rank (MWR) tests, as implemented in Sigmastat for Windows version 2.0, Jandel Corporation. No corrective algorithms were employed.

Electron microscopy (EM)

Eight μl of sample were spotted onto a glow-discharged, carbon-coated Formvar grid (Electron Microscopy Sciences, Hatfield, PA) and incubated for 10 min. The solution then was gently wicked off using Whatman Grade 2 filter paper. The samples were fixed with 5 μl of 2.5% (v/v) glutaraldehyde for 5 min, after which the glutaraldehyde solution was wicked off. The grid then was stained with 5 μl of 1% (w/v) filtered (0.2 μm) aqueous uranyl acetate (Ted Pella Inc, Redding, CA) for 5 min. After careful removal of staining solutions with filter paper, the grids were air dried. Four independent experiments were carried out for each peptide. Grids were visualized using a JEOL JEM CX 100 II transmission electron microscope (JEOL, Peabody, MA).

Cross-linking and SDS-PAGE analysis

Peptides were covalently cross-linked, using the technique of photo-induced cross-linking of unmodified proteins (PICUP) [26], immediately after their solvation from lyophilizates [27]. Briefly, 1 μl of 1 mM Tris(2,2′-bipyridyl)dichlororuthenium(II) and 1 μl of 20 mM ammonium persulfate in 10 mM sodium phosphate, pH 7.4, were added to 18 μl of a 20–30 μM solution of Aβ or its mutants. The mixture was irradiated for 1 s with visible light and the reaction was quenched immediately with 10 μl of 5% (v/v) β-mercaptoethanol in tricine sample buffer (Invitrogen, Carlsbad, CA). The cross-linked oligomer mixtures were fractionated by SDS-PAGE using 10–20% Tricine gels (1.0 mm × 10 well) (Invitrogen) and then silver stained using a SilverXpress silver staining kit (Invitrogen). The amounts taken for SDS-PAGE analyses were adjusted according to the peptide concentration, determined by amino acid analysis, so that equal amounts of protein were loaded in each lane. Gels were scanned using a CanoScan 9950F scanner (Canon, Chesapeake, VA). The intensities of each band were analyzed by densitometry using the public domain NIH Image program (http://rsbweb.nih.gov/nih-image/).

RESULTS

Secondary structure dynamics

Aβ has been shown to exist predominantly as a statistical coil (SC) immediately after solvation of peptide lyophilizates in biological buffers under conditions designed to prevent peptide self-assembly [28]. To monitor the secondary structures of [ΔE22]Aβ peptides immediately after their solvation, and during peptide assembly, CD was performed (Fig. 1). The CD spectra were consistent with the existence of predominately SC conformers of Aβ40, Aβ42, and [ΔE22]Aβ40, as indicated by negative molar ellipticities at ≈198 nm. The conformers of [ΔE22]Aβ42 contained predominately β-sheet secondary structure elements, as indicated by the large magnitude minimum centered at ≈218 nm. Incubation of the former three peptides at 37°C without agitation resulted in a SC→β-sheet transition that exhibited

an isodichroic point between ≈208–210 nm (Figs. 1 A–C, arrows). This transition began after ≈5 d for Aβ40. The midpoint of the transition was ≈8 d. A classical β-sheet spectrum, with a negative ellipticity centered at ≈217 nm, was observed by day 14. In contrast, the SC→β-sheet transition in [ΔE22]Aβ40 occurred within 2 h, with a transition midpoint at ≈30 min, ≈400-fold faster than observed with Aβ40. Aβ42 displayed a SC→β-sheet transition in 48 h that was qualitatively similar to that of Aβ40, but with accelerated kinetics and with a transition midpoint at ≈24 h. No transition was observed for [ΔE22]Aβ42, which existed *initially* as a β-sheet-rich conformer and remained in this state during the entire experiment.

Cosolvent and solvent effects on secondary structure

The solvophobic behavior of the peptide backbone in the presence of cosolvents like TFE and HFIP facilitates α-helix formation [29, 30]. However, the amount of α-helix formed at specific cosolvent concentrations depends on the primary structure and native higher-order structure of the protein [30]. Stable protein folds containing non-helical segments have lower propensities for α-helix formation than do folds of lower stability. The cosolvent concentration-dependence for α-helix formation thus can reveal relative differences in conformational stability among different proteins.

We began our studies by monitoring the secondary structure of the WT and ΔE22 peptides in the presence of the cosolvent TFE. Aβ peptides were suspended in TFE in 10 mM sodium phosphate, pH 7.4, and analyzed immediately by CD (Fig. 2). A SC→α-helix transition was observed in WT Aβ40 and Aβ42 peptides as the TFE concentration increased. For [ΔE22]Aβ40, as the TFE concentration increased from 0→15%, a SC→β-sheet transition was observed. Further increases in TFE concentration produced increasing levels of α-helix. [ΔE22]Aβ42 initially exhibited pronounced β-sheet structure (≈52%). Increases in TFE concentration did produce increased α-helix content, but even at 60% TFE, β-sheet content was ≈40%, whereas α-helix was only ≈23%. For all peptides, the spectra obtained with 70–90% TFE overlapped with those obtained with 60% TFE (data not shown). At 100% TFE, all four peptides showed typical α-helix spectra with a maximum at ≈192 nm and double minima at ≈208 and ≈220 nm (Fig. S1).

To complement the TFE studies, we studied the effects of the cosolvent hexafluoroisopropanol (HFIP), a stronger helix-inducing co-solvent [31]. Each of the WT and [ΔE22] Aβ peptides were dissolved in neat HFIP and then added to a mixture of 10 mM sodium phosphate, pH 7.4, and HFIP to obtain 5%→100% (v/v) HFIP (for 0%, HFIP was evaporated from each sample and then buffer was added). With increasing HFIP concentration, two transitions were observed (Fig. S2). At HFIP concentrations up to 10%, a SC→β-sheet transition was observed for all the peptides, except for [ΔE22]Aβ42, which existed initially as a β-sheet conformer. From 20–90% HFIP, increasing α-helix content, signified by double minima at ≈207 and ≈219 nm, was evident. At 100% HFIP, minima with lower absolute intensities were observed, and the first minimum was shifted to ≈204 from ≈207. All peptides were fully α-helical under this condition.

Alkaline pH has been shown to increase the solubility of Aβ peptides and decrease *de novo* peptide aggregation [22, 28]. To determine if differential effects of alkaline pH on secondary structure occurred among the study peptides, we dissolved the peptides in 10 mM sodium phosphate, at either pH 10 or 12. At pH 10, the Aβ40 peptides displayed SC conformations (Fig. S3). [ΔE22]Aβ40 displayed a mixture of SC and β-sheet, as indicated by a negative peak at ≈198 nm and a shoulder at ≈217 nm, whereas [ΔE22]Aβ42 was largely β-sheet. At pH 12, all the peptides produced spectra consistent with SC conformation. However, the spectra of both ΔE22 peptides displayed decreased [Θ] in the region ≈210– 230 nm relative to their WT analogues.

Fibril nucleation and elongation

To probe the kinetics of fibril formation, ThT fluorescence was measured periodically during incubation of WT and mutant Aβ peptides. The peptides were dissolved in 10 mM phosphate buffer, pH 7.4, and incubated at 37°C. ThT fluorescence does not measure fibril concentration *per se* (fibrils of some proteins do not produce typical ThT fluorescence) [32], but fluorescence intensities do correlate with Aβ fibril content [33]. Aβ40 displayed a sigmoidal process curve characterized by a lag time of ≈100 h, which was followed by a monotonic increase in ThT fluorescence that plateaued after ≈240 h (Fig. 3A). In contrast, [ΔE22]Aβ40 displayed no lag phase, but exhibited a rapid increase in ThT fluorescence that reached maximal levels by ≈72 h. In an assembly reaction in which freshly prepared [ΔE22]Aβ40 was mixed with Aβ40 in a 1:10 molar ratio, we observed a hyperbolic increase in ThT fluorescence with no lag phase. Maximal fluorescence levels were reached after ≈120 h. Relative rates of ThT fluorescence change were [ΔE22]Aβ40 > [ΔE22]Aβ40:Aβ40 (1:10) > Aβ40. Similar results were obtained with Aβ42 peptides in that the relative rates of ThT fluorescence increase were [ΔE22]Aβ42 >> [ΔE22]Aβ42:Aβ42 (1:10) > Aβ42 (Fig. 3B). Immediately after dissolution, [ΔE22]Aβ42 displayed high ThT fluorescence that trended towards higher intensities with time, but this trend was statistically insignificant. The [ΔE22]Aβ42:Aβ42 and Aβ42 samples produced hyperbolic progress curves that reached maximal ThT fluorescence levels at ≈24 h and ≈48 h, respectively. In each of these cases, no lag phases were observed.

Peptide oligomerization

To determine peptide oligomerization state, peptides were subjected to photochemical cross-linking (PICUP) immediately after their preparation from lyophilizates and then the covalently stabilized peptides were fractionated by SDS-PAGE. This method accurately determines the oligomer size distribution for low-order Aβ oligomers [26, 27].

Un-cross-linked WT Aβ40 and [ΔE22]Aβ40 each displayed predominately a single band at the M_r of monomer (Fig. 4, lanes 1 and 2, respectively). A very faint dimer also was observed. Cross-linking of Aβ40 (Fig. 4, lane 3) produced the characteristic distributions of oligomers [34], comprising bands corresponding to monomer through tetramer. Cross-linked [ΔE22]Aβ40 (Fig. 4, lane 4) displayed a distribution comprising monomers to tetramers that included a weakly staining tetramer band that appeared to have greater electrophoretic mobility than its WT homologue (Table 2).

Un-cross-linked WT Aβ42 and [ΔE22]Aβ42 samples produced monomers and trimers (Fig. 4, lanes 5 and 6, respectively). The trimer band in Aβ42 has been shown to be induced by SDS [34]. Cross-linked WT Aβ42 produced bands corresponding to monomer through heptamer, with an intensity node in the tetramer-pentamer region (Fig. 4, lane 7). [ΔE22]Aβ42 (Fig. 4, lane 8) produced a band intensity profile in which significantly more higher-order oligomers were observed. The relative amounts of monomers and dimers in this sample were lower than in the WT sample and the intensities of the bands in the trimer-heptamer range were greater. In addition, bands at higher M_r (>30 kDa) were observed.

Morphologic analysis of assemblies

Electron microscopy was used to determine the morphologies of the assemblies formed by the four different Aβ peptides immediately after dissolution of the respective lyophilizates. Aβ40 displayed a variety of assemblies, including globular, multi-globular, and nebulous structures. Diameters of these structures ranged from ≈5–25 nm (Fig. 5A). Aβ42 produced a mixture of globular and short filamentous structures (Fig. 5B). The globular structures ranging from ≈5–10 nm. Filaments of width ≈4–5 nm and length ≈40–60 nm were observed. Unlike WT Aβ, [ΔE22]Aβ40 formed short, relatively straight filaments that were

≈7–9 nm wide and ≈80–120 nm long (Fig 5C, blue arrow). Multi-stranded (Fig 5C, black arrow), and some thin filaments (≈4–5 nm wide) (Fig 5C, white arrowhead), also were observed. [ΔE22]Aβ42 produced twisted thread-like or protofibril-like structures of ≈6-8 nm in width (Fig 5D). The average length of these structures was ≈60-120 nm.

Peptides were incubated and then re-examined after structural changes in the peptides ceased to occur, as determined by the observation of constant ThT fluorescence and CD spectra. At this point, all four peptides existed as long, unbranched fibrils with smooth margins (Fig. 5E-H). Aβ40 produced bifilar structures (Fig. 5E, dark blue arrow) of 8–14 nm in diameter that displayed helical twists with pitches of ≈200 nm (Fig. 5E, black arrow). Aβ42 formed fibrils that were morphologically similar to Aβ40, with widths of 7–11 nm (Fig. 5F, black arrow). Some of the fibrils appeared to be double stranded with helical twists (Fig. 5F, dark blue arrow). [ΔE22]Aβ40 formed non-branched, straight (Fig. 5G, white arrow), curved (Fig. 5G, black arrow-head), and some twisted (Fig. 5G, dark blue arrow) filaments with diameters of 9–11 nm. [ΔE22]Aβ42 produced bifilar structures with diameters ≈9 nm. These assemblies displayed irregular or helical twists with pitches of ≈40–80 nm (Fig. 5H).

Fibril stability

One measure of fibril stability is the critical concentration (C_r), the monomer concentration in a fibril assembly reaction at equilibrium. We determined the C_r for the four study peptides by incubating them at 37°C, without agitation, until maximal ThT fluorescence was observed. We then performed quantitative amino acid analysis of supernates obtained by centrifugation at 436,000 × g for 1 h. The C_r values thus obtained are shown in Table 1. [ΔE22]Aβ40 had a C_r (0.58 μM) that was significantly ($p < 0.001$) lower than that of WT Aβ40 (1.24 μM). Similarly, the C_r of [ΔE22]Aβ42 (0.32 μM) was significantly ($p = 0.003$) lower than that of WT Aβ42 (0.87 μM). Both C_r values for the ΔE22 peptides were significantly lower than the WT peptide C_r values (e.g., $p < 0.004$ for the difference between the most stable WT Aβ peptide, Aβ42, and the least stable ΔE22 peptide, [ΔE22]Aβ40).

Because the C_r is directly related to the Gibbs free energy for the Aβ ⇌ fibril equilibrium, by the relationship $\Delta G^0 = -RT\ ln\ (1/C_r)$, we used this relationship to determine the magnitudes of the stability differences we observed (see Materials and Methods). The ΔG^0 values ranged from –9.23 to –8.38 kcal/mol (Table 1).

DISCUSSION

Genetic forms of disease provide the opportunity to identify the causative mutation(s), and in the case of a mutation within a protein coding region, to study the properties of the resultant mutant protein and attempt to relate these properties to disease mechanism. In AD, familial forms of the disease may arise from mutations affecting the absolute amounts of Aβ produced, the relative amounts of Aβ40, Aβ42, or Aβ peptides of other lengths, or the Aβ peptide sequence. A recently discovered FAD mutation in a family in Osaka, Japan, results in the production of Aβ peptides lacking Glu22 (ΔE22), [18]. Initial studies seeking to determine the effect of this deletion on the biophysical behavior of the peptide suggested that the Osaka form of Aβ did not form fibrils *in vitro*, although it did form oligomers, and that patients from the Osaka family did not have amyloid plaques [18]. [ΔE22]Aβ inhibited hippocampal long-term potentiation (LTP) in rats and caused synapse loss in mouse hippocampal slices, although little effect was observed in MTT assays [18, 35]. Subsequent studies reported the identification of ΔE22Aβ oligomers in transfected cells, based on immunoreactivity with the ADDL-specific antibody NU1 [36].

Our interest in the Osaka peptide was stimulated by the fact that Glu22 plays an important role in controlling Aβ monomer folding and subsequent peptide self-association [19, 20, 37-41], and thus its elimination would be expected to have significant effects on these processes. Such effects have been observed in studies of Aβ mutants containing amino acid substitutions for Glu22 [20]. The results of our studies of the ΔE22 forms of Aβ40 and Aβ42 show, contrary to prior published work, that elimination of Glu22 causes an extraordinary increase in the propensity of Aβ to form fibrils. We use the term "extraordinary" because the magnitude of the kinetic alteration, especially in the case of [ΔE22]Aβ42, was so great that fibril formation occurred during the initial solvation of the peptide.

It is possible that the prior failure to observe significant ThT fluorescence in [ΔE22]Aβ40 or [ΔE22]Aβ42 peptides [18] may have been due to loss of protein by simple precipitation, as these experiments were done using a relatively high Aβ concentration (100 μM) and in a solvent, PBS, in which relatively rapid fibril formation occurs with even WT peptides. In our initial experiments, we encountered this phenomenon (data not shown) and were able to recognize it only by careful monitoring of protein concentration at each step of the experiments. Differences in peptide preparation methods also may have contributed to the different experimental results. Tomiyama *et al.* [18] prepared their peptides using hexafluoroisopropanol solvation, evaporation, and ammonium hydroxide solubilization. A 1:9 (v/v; peptide:PBS) dilution then was made prior to certain experimental studies. Hexafluroisopropanol solvation, evaporation, DMSO solubilization, and PBS dilution was employed in other experiments. In addition to the distinct preparation procedures, the system of Tomiyama *et al.* differs from ours in the presence of the ammonium cation or DMSO in the final PBS solution used for the experiments.

We began our studies by examining the time evolution of secondary structure. Consistent with prior studies [42-44], Aβ40, Aβ42 and [ΔE22]Aβ40 existed predominately as statistical coils immediately after solvation, but all then displayed SC→β-sheet transitions. Remarkably, [ΔE22]Aβ40 underwent this transition ≈400-fold faster than did its WT homologue. [ΔE22]Aβ42 did not display such a transition at all, but rather possessed a level of β-sheet equivalent to that observed after fibril formation. The relative kinetics of secondary structure changes among the peptides was maintained in ThT fluorescence experiments. WT Aβ40 displayed lag and growth phases, whereas WT Aβ42 and [ΔE22]Aβ40 displayed no lag phases. [ΔE22]Aβ42 displayed no substantial transition in ThT fluorescence intensity, but rather exhibited high ThT fluorescence when the initial measurement was made.

The most significant factor contributing to the acceleration of Aβ40 assembly was diminution of the lag phase, which suggests that the Glu22 deletion facilitates the folding of the Aβ monomer into a conformer with a high propensity to self-associate into fibril nuclei. The effect of the Glu22 deletion in the Aβ42 system was primarily on overall fibril formation kinetics because no lag phases were observed. This observation is consistent with experimental and computational studies that have demonstrated that Aβ42 possesses greater initial structural order than does Aβ40 [19, 20, 34, 45-47].

We reported previously that Aβ40, Aβ42, and all reported mutant or truncated forms of these two peptides undergo a SC→α-helix→β-sheet conformational transition during assembly from nascent monomer to fibril [44]. Fluorinated alcohols (TFE or HFIP) affected the kinetics of these conformational transitions, and thus the kinetics of peptide assembly, through their ability to stabilize helical forms of the peptides [48]. The stabilization of α-helices depended not only on the intrinsic propensity of the peptide backbone to adopt helical states, due to its solvophobicity in fluorinated alcohols, but also on the primary

structure-dependence of α-helix stability [30]. Here, we probed the effect of the ΔE22 primary structure change on peptide conformational stability by determining the secondary structure content of Aβ40, Aβ42, and their ΔE22 homologues in different concentrations of fluorinated alcohols. In the Aβ40 system, increasing concentrations of TFE produced a SC→α-helix transition in the WT peptide. In contrast, a SC→β-sheet→α-helix transition occurred with the ΔE22 peptide. In kinetic studies of WT Aβ fibril formation, a SC→α-helix transition occurs obligatorily *before* β-sheet formation [44, 48]. For this reason, low concentrations of TFE accelerate fibril formation by accelerating this initial conformational transition. The lack of an observed α-helix state in the [ΔE22]Aβ40 peptide at low TFE concentrations suggests that the ΔE22 mutation increases the peptide's propensity for β-sheet formation so significantly that the SC→α-helix transition occurs too quickly to be monitored in the experimental system employed. Higher concentrations of TFE block the α-helix→β-sheet transition, and hence fibril formation, by increasing the activation energy for the transition or by decreasing the free energy of the α-helix state [48]. Consistent with this observation, higher TFE concentrations did result in α-helix formation in the [ΔE22]Aβ40 peptide. The effect of the ΔE22 mutation on Aβ40 was so large that the behavior of the mutant peptide was similar to that of WT Aβ42. Not surprisingly, the propensity of the ΔE22 variant of Aβ42 for β-sheet formation was so high that no α-helix conformer could be observed at low TFE concentration and no such conformer was formed up to 60% TFE. An α-helix state *was* observed when 100% TFE was used. Qualitatively similar data were obtained using HFIP, with the one exception that α-helix was observed in [ΔE22]Aβ42 when the HFIP concentration reached 20%. The rank order of β-sheet propensity, [ΔE22]Aβ42 >> Aβ42 > [ΔE22]Aβ40 > Aβ40, also was observed in studies of the effect of pH 10 and pH 12 on conformation. In these experiments, the latter two peptides largely existed in SC form. [ΔE22]Aβ40 displayed a β-sheet element, whereas [ΔE22]Aβ42 was largely β-sheet. Taken together, the results of these three experiments support a conclusion that the ΔE22 mutation substantially increases peptide β-sheet propensity in Aβ40 and produces β-sheet structure of extraordinary stability in [ΔE22]Aβ42.

Conformational and kinetics differences among the peptides were mirrored by their oligomerization states. [ΔE22]Aβ40 had a more restricted distribution than did WT Aβ40, one in which the largest predominant oligomer was trimer instead of tetramer. The molecular basis for this observation is unclear. In addition, the [ΔE22]Aβ40 oligomers all displayed electrophoretic mobilities greater than those of their WT homologues. The simplest explanation for this difference is the 128 molecular weight decrement in the mutant peptides. However, it also is possible that the mutant oligomers have more compact structures or bind different amounts of SDS.

The largest differences in oligomerization were seen in the [ΔE22]Aβ42 peptides, which showed higher propensities for oligomerization. Increased oligomer frequencies were observed in the region corresponding to paranuclei [34]. In addition, higher-order oligomers (dodecamer and octadecamer regions) were observed in the [ΔE22]Aβ42 samples that were not seen at all in the WT samples. The accelerated conformational and assembly kinetics displayed by the mutant peptides thus correlates with an increased oligomerization propensity. Not surprisingly, the rapid early kinetics also was reflected in rapid fibril formation. Whereas both WT Aβ40 and Aβ42 peptides possessed nebulous globular and very short irregular string-like morphologies immediately upon solvation from lyophilizates, short protofibrillar and fibrillar structures were evident immediately in the ΔE22 samples.

A kinetic effect of the ΔE22 mutation also was supported by the results of measurement of the C_r for each of the four peptides. These values ranged from 0.32–1.24 μM, consistent with values reported before for Aβ40 in PBS [49, 50]. To the nearest 0.5 μM, the C_r values of the ΔE22 peptides were ≈1/2 those of the respective WT peptides. Using these C_r data,

ΔG^0 calculations revealed that the stability of the fibrils formed by each ΔE22 peptide was ≈0.5 kcal/mol larger than its respective WT homologue. This small stability increase, less than a single H-bond, is too low to account for the observed rate differences in CD spectral changes, increases in ThT fluorescence, and fibril evolution. We conclude that the primary effect of the ΔE22 mutation is to stabilize β-structure within the Aβ monomer or within low-order oligomers, which results in an extraordinary change in the kinetics of fibril formation without producing a change of equivalent magnitude in system thermodynamics (i.e., fibril stability). This mechanism is consistent with prior experimental and computational studies of the kinetics and thermodynamics of Aβ fibril formation that suggest that monomer conformational rearrangement is a rate-limiting step in fibril elongation [51-53].

Supplementary Material

Refer to Web version on PubMed Central for supplementary material.

Acknowledgments

We thank Margaret M. Condron for technical assistance.

Abbreviations

Aβ	amyloid β-protein
AAA	amino acid analysis
AD	Alzheimer disease
APP	amyloid β-protein precursor
CAA	cerebral amyloid angiopathy
CD	circular dichroism spectroscopy
C_r	critical concentration
ΔE22	deletion of Glu22
EM	electron microscopy
FAD	familial AD
HFIP	1,1,1,3,3,3-hexafluoro-2-propanol
PICUP	photo-induced cross-linking of unmodified proteins
RP-HPLC	reverse-phase high-performance liquid chromatography
Ru(bpy)	tris(2,2′-bipyridyl)dichlororuthenium(II) hexahydrate
SC	statistical coil
SDS-PAGE	sodium dodecyl sulfate-polyacrylamide gel electrophoresis
TFE	2,2,2-trifluoroethanol
ThT	thioflavin T
WT	wild type

REFERENCES

1. Prusiner SB. Shattuck lecture - Neurodegenerative diseases and prions. New England Journal of Medicine. 2001; 344:1516–1526. [PubMed: 11357156]
2. Vinters HV, Wang ZZ, Secor DL. Brain parenchymal and microvascular amyloid in Alzheimer's disease. Brain Pathol. 1996; 6:179–195. [PubMed: 8737932]
3. Goedert M, Spillantini MG. A century of Alzheimer's disease. Science. 2006; 314:777–781. [PubMed: 17082447]
4. Hardy JA, Higgins GA. Alzheimer's disease: the amyloid cascade hypothesis. Science. 1992; 256:184–185. [PubMed: 1566067]
5. Roychaudhuri R, Yang M, Hoshi MM, Teplow DB. Amyloid β-protein assembly and Alzheimer disease. J Biol Chem. 2009; 284:4749–4753. [PubMed: 18845536]
6. Ono K, Condron MM, Teplow DB. Structure-neurotoxicity relationships of amyloid β-protein oligomers. Proc Natl Acad Sci U S A. 2009; 106:14745–14750. [PubMed: 19706468]
7. Janssen JC, Beck JA, Campbell TA, Dickinson A, Fox NC, Harvey RJ, et al. Early onset familial Alzheimer's disease: Mutation frequency in 31 families. Neurology. 2003; 60:235–239. [PubMed: 12552037]
8. Wakutani Y, Watanabe K, Adachi Y, Wada-Isoe K, Urakami K, Ninomiya H, et al. Novel amyloid precursor protein gene missense mutation (D678N) in probable familial Alzheimer's disease. J Neurol Neurosurg Psychiatry. 2004; 75:1039–1042. [PubMed: 15201367]
9. Hendriks L, van Duijn CM, Cras P, Cruts M, Van Hul W, van Harskamp F, et al. Presenile dementia and cerebral haemorrhage linked to a mutation at codon 692 of the β-amyloid precursor protein gene. Nat Genet. 1992; 1:218–221. [PubMed: 1303239]
10. Levy E, Carman MD, Fernandez-Madrid IJ, Power MD, Lieberburg I, van Duinen SG, et al. Mutation of the Alzheimer's disease amyloid gene in hereditary cerebral hemorrhage, Dutch type. Science. 1990; 248:1124–1126. [PubMed: 2111584]
11. Van Broeckhoven C, Haan J, Bakker E, Hardy JA, Van Hul W, Wehnert A, et al. Amyloid β protein precursor gene and hereditary cerebral hemorrhage with amyloidosis (Dutch). Science. 1990; 248:1120–1122. [PubMed: 1971458]
12. Rossi G, Macchi G, Porro M, Giaccone G, Bugiani M, Scarpini E, et al. Fatal familial insomnia: genetic, neuropathologic, and biochemical study of a patient from a new Italian kindred. Neurology. 1998; 50:688–692. [PubMed: 9521257]
13. Kamino K, Orr HT, Payami H, Wijsman EM, Alonso ME, Pulst SM, et al. Linkage and mutational analysis of familial Alzheimer disease kindreds for the APP gene region. Am J Hum Genet. 1992; 51:998–1014. [PubMed: 1415269]
14. Nilsberth C, Westlind-Danielsson A, Eckman CB, Condron MM, Axelman K, Forsell C, et al. The 'Arctic' APP mutation (E693G) causes Alzheimer's disease by enhanced Aβ protofibril formation. Nat Neurosci. 2001; 4:887–893. [PubMed: 11528419]
15. Grabowski TJ, Cho HS, Vonsattel JP, Rebeck GW, Greenberg SM. Novel amyloid precursor protein mutation in an Iowa family with dementia and severe cerebral amyloid angiopathy. Ann Neurol. 2001; 49:697–705. [PubMed: 11409420]
16. Selkoe DJ, Podlisny MB. Deciphering the genetic basis of Alzheimer's disease. Annu Rev Genomics Hum Genet. 2002; 3:67–99. [PubMed: 12142353]
17. Yamada M. Cerebral amyloid angiopathy: an overview. Neuropathology. 2000; 20:8–22. [PubMed: 10935432]
18. Tomiyama T, Nagata T, Shimada H, Teraoka R, Fukushima A, Kanemitsu H, et al. A new amyloid β variant favoring oligomerization in Alzheimer's-type dementia. Ann Neurol. 2008; 63:377–387. [PubMed: 18300294]
19. Lazo ND, Grant MA, Condron MC, Rigby AC, Teplow DB. On the nucleation of amyloid β-protein monomer folding. Protein Sci. 2005; 14:1581–1596. [PubMed: 15930005]
20. Grant MA, Lazo ND, Lomakin A, Condron MM, Arai H, Yamin G, et al. Familial Alzheimer's disease mutations alter the stability of the amyloid β-protein monomer folding nucleus. Proc Natl Acad Sci U S A. 2007; 104:16522–16527. [PubMed: 17940047]

21. Walsh DM, Lomakin A, Benedek GB, Condron MM, Teplow DB. Amyloid β-protein fibrillogenesis. Detection of a protofibrillar intermediate. J Biol Chem. 1997; 272:22364–22372. [PubMed: 9268388]
22. Fezoui Y, Hartley DM, Harper JD, Khurana R, Walsh DM, Condron MM, et al. An improved method of preparing the amyloid β-protein for fibrillogenesis and neurotoxicity experiments. Amyloid. 2000; 7:166–178. [PubMed: 11019857]
23. Lomakin A, Chung DS, Benedek GB, Kirschner DA, Teplow DB. On the nucleation and growth of amyloid β-protein fibrils: detection of nuclei and quantitation of rate constants. Proc Natl Acad Sci U S A. 1996; 93:1125–1129. [PubMed: 8577726]
24. Andreu JM, Timasheff SN. The measurement of cooperative protein self-assembly by turbidity and other techniques. Methods in Enzymology. 1986; 130:47–59. [PubMed: 3773745]
25. O'Nuallain B, Shivaprasad S, Kheterpal I, Wetzel R. Thermodynamics of Aβ(1-40) amyloid fibril elongation. Biochemistry. 2005; 44:12709–12718. [PubMed: 16171385]
26. Bitan G, Teplow DB. Rapid photochemical cross-linking--a new tool for studies of metastable, amyloidogenic protein assemblies. Acc Chem Res. 2004; 37:357–364. [PubMed: 15196045]
27. Bitan G, Lomakin A, Teplow DB. Amyloid β-protein oligomerization: prenucleation interactions revealed by photo-induced cross-linking of unmodified proteins. J Biol Chem. 2001; 276:35176–35184. [PubMed: 11441003]
28. Teplow DB. Preparation of amyloid β-protein for structural and functional studies. Methods Enzymol. 2006; 413:20–33. [PubMed: 17046389]
29. Kentsis A, Sosnick TR. Trifluoroethanol promotes helix formation by destabilizing backbone exposure: desolvation rather than native hydrogen bonding defines the kinetic pathway of dimeric coiled coil folding,. Biochemistry. 1998; 37:14613–14622. [PubMed: 9772190]
30. Buck M. Trifluoroethanol and colleagues: cosolvents come of age. Recent studies with peptides and proteins. Q Rev Biophys. 1998; 31:297–355. [PubMed: 10384688]
31. Barrow CJ, Yasuda A, Kenny PT, Zagorski MG. Solution conformations and aggregational properties of synthetic amyloid β-peptides of Alzheimer's disease. Analysis of circular dichroism spectra. J Mol Biol. 1992; 225:1075–1093. [PubMed: 1613791]
32. Groenning M. Binding mode of Thioflavin T and other molecular probes in the context of amyloid fibrils—current status. Journal of Chemical Biology. 2010; 3:1–18. [PubMed: 19693614]
33. LeVine H 3rd. Quantification of β-sheet amyloid fibril structures with thioflavin T. Methods Enzymol. 1999; 309:274–284. [PubMed: 10507030]
34. Bitan G, Kirkitadze MD, Lomakin A, Vollers SS, Benedek GB, Teplow DB. Amyloid beta - protein (Aβ) assembly: Aβ40 and Aβ42 oligomerize through distinct pathways. Proc Natl Acad Sci U S A. 2003; 100:330–335. [PubMed: 12506200]
35. Takuma H, Teraoka R, Mori H, Tomiyama T. Amyloid-β E22Δvariant induces synaptic alteration in mouse hippocampal slices. NeuroReport. 2008; 19:615–619. 610.1097/WNR. 1090b1013e3282fb1078c1094. [PubMed: 18382273]
36. Nishitsuji K, Tomiyama T, Ishibashi K, Ito K, Teraoka R, Lambert MP, et al. The E693Δ mutation in amyloid precursor protein increases intracellular accumulation of amyloid β oligomers and causes endoplasmic reticulum stress-induced apoptosis in cultured cells. Am J Pathol. 2009; 174:957–969. [PubMed: 19164507]
37. Baumketner A, Bernstein SL, Wyttenbach T, Lazo ND, Teplow DB, Bowers MT, et al. Structure of the 21-30 fragment of amyloid β-protein. Protein Sci. 2006; 15:1239–1247. [PubMed: 16731963]
38. Peralvarez-Marin A, Mateos L, Zhang C, Singh S, Cedazo-Minguez A, Visa N, et al. Influence of residue 22 on the folding, aggregation profile, and toxicity of the Alzheimer's amyloid β peptide. Biophys J. 2009; 97:277–285. [PubMed: 19580765]
39. Fawzi NL, Kohlstedt KL, Okabe Y, Head-Gordon T. Protofibril assemblies of the arctic, Dutch, and Flemish mutants of the Alzheimer's Aβ1-40 peptide. Biophys J. 2008; 94:2007–2016. [PubMed: 18032553]
40. Lam AR, Teplow DB, Stanley HE, Urbanc B. Effects of the Arctic (E22→G) mutation on amyloid β-protein folding: discrete molecular dynamics study. J Am Chem Soc. 2008; 130:17413–17422. [PubMed: 19053400]

41. Melchor JP, McVoy L, Van Nostrand WE. Charge alterations of E22 enhance the pathogenic properties of the amyloid β-protein. J Neurochem. 2000; 74:2209–2212. [PubMed: 10800967]
42. Maji SK, Amsden JJ, Rothschild KJ, Condron MM, Teplow DB. Conformational dynamics of amyloid β-protein assembly probed using intrinsic fluorescence. Biochemistry. 2005; 44:13365–13376. [PubMed: 16201761]
43. Maji SK, Ogorzalek Loo RR, Inayathullah M, Spring SM, Vollers SS, Condron MM, et al. Amino acid position-specific contributions to amyloid β-protein oligomerization. J Biol Chem. 2009; 284:23580–23591. [PubMed: 19567875]
44. Kirkitadze MD, Condron MM, Teplow DB. Identification and characterization of key kinetic intermediates in amyloid β-protein fibrillogenesis. J Mol Biol. 2001; 312:1103–1119. [PubMed: 11580253]
45. Yang M, Teplow DB. Amyloid β-protein monomer folding: free-energy surfaces reveal alloform-specific differences. J Mol Biol. 2008; 384:450–464. [PubMed: 18835397]
46. Teplow DB, Lazo ND, Bitan G, Bernstein S, Wyttenbach T, Bowers MT, et al. Elucidating amyloid β-protein folding and assembly: A multidisciplinary approach. Acc Chem Res. 2006; 39:635–645. [PubMed: 16981680]
47. Sgourakis NG, Yan Y, McCallum SA, Wang C, Garcia AE. The Alzheimer's peptides Aβ40 and 42 adopt distinct conformations in water: a combined MD / NMR study. J Mol Biol. 2007; 368:1448–1457. [PubMed: 17397862]
48. Fezoui Y, Teplow DB. Kinetic studies of amyloid β-protein fibril assembly. Differential effects of α-helix stabilization. J Biol Chem. 2002; 277:36948–36954. [PubMed: 12149256]
49. Williams AD, Portelius E, Kheterpal I, Guo JT, Cook KD, Xu Y, et al. Mapping Aβ amyloid fibril secondary structure using scanning proline mutagenesis. J Mol Biol. 2004; 335:833–842. [PubMed: 14687578]
50. Williams AD, Shivaprasad S, Wetzel R. Alanine scanning mutagenesis of Aβ(1-40) amyloid fibril stability. J Mol Biol. 2006; 357:1283–1294. [PubMed: 16476445]
51. Kusumoto Y, Lomakin A, Teplow DB, Benedek GB. Temperature dependence of amyloid β-protein fibrillization. Proc Natl Acad Sci U S A. 1998; 95:12277–12282. [PubMed: 9770477]
52. Esler WP, Stimson ER, Jennings JM, Vinters HV, Ghilardi JR, Lee JP, et al. Alzheimer's disease amyloid propagation by a template-dependent dock-lock mechanism. Biochemistry. 2000; 39:6288–6295. [PubMed: 10828941]
53. Massi F, Straub JE. Energy landscape theory for Alzheimer's amyloid β-peptide fibril elongation. Proteins: Structure, Function, & Genetics. 2001; 42:217–229.

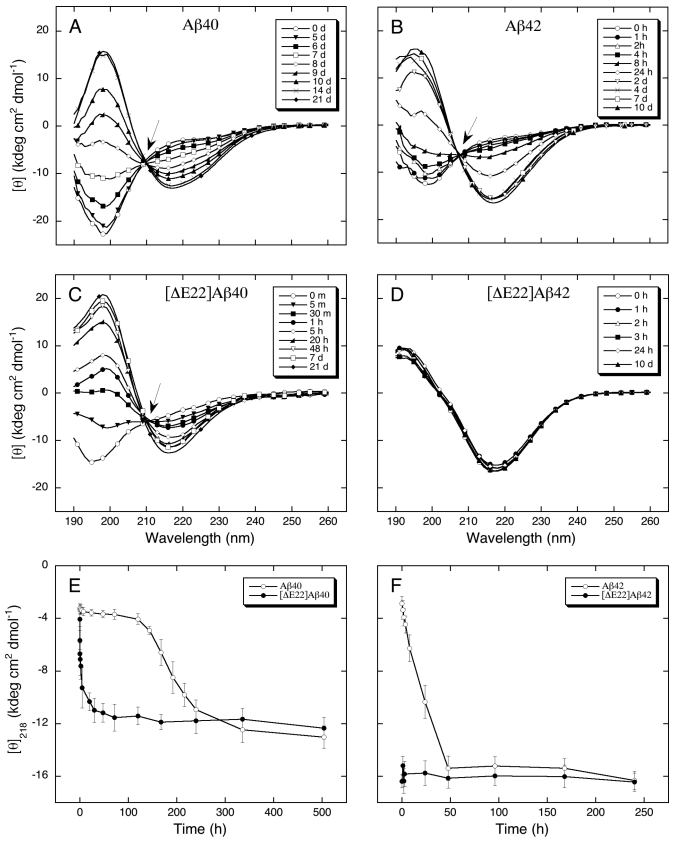

Figure 1.

Secondary structure dynamics. (A) Aβ40, (B) Aβ42, (C) [ΔE22]Aβ40 and (D) [ΔE22]Aβ42 were incubated at 37°C in 10 mM phosphate buffer, pH 7.4. Spectra were acquired immediately at the start of the incubation period. Text boxes show times of spectral acquisition (m, min; h, hours; or d, days). Arrows indicate isodichroic points. Spectra presented for peptides are representative of those obtained in each of four independent experiments. Molar ellipticity $[\Theta]_{218}$ at various time points for (E) Aβ40 (-○-), (E) [ΔE22]Aβ40 (-●-), (F) Aβ42 (-○-) and (F) [ΔE22]Aβ42 (-●-).

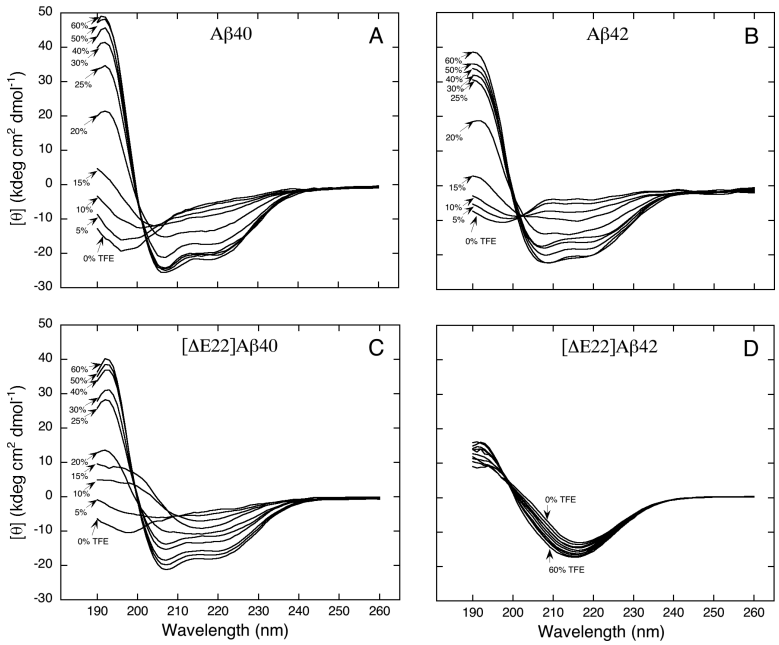

Figure 2.

Cosolvent effect on secondary structure. CD spectra of (A) Aβ40, (B) Aβ42, (C) [ΔE22]Aβ40 and (D) [ΔE22]Aβ42 in 10 mM phosphate buffer, pH 7.4, and varying concentrations (v/v) of TFE (as indicated), were recorded at 23°C. Spectra presented are representative of four independent experiments.

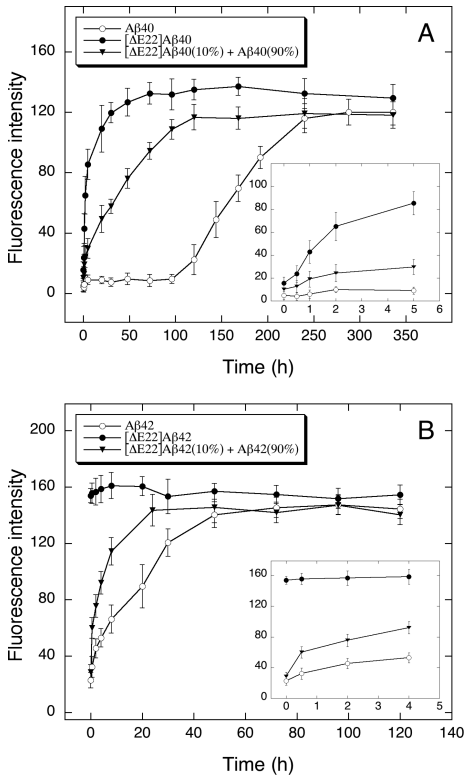

Figure 3.

Thioflavin T binding. (A) Aβ40 (-○-), (A) [ΔE22]Aβ40 (-●-), (B) Aβ42 (-○-) and (B) [ΔE22]Aβ42 (-●-) were incubated at 37°C in 10 mM phosphate buffer, pH 7.4. Periodically, aliquots were removed and ThT binding levels were determined. Nucleation activity of [ΔE22]Aβ peptides was assessed by addition of (A) 10% (v/v) of [ΔE22]Aβ40 to 90% (v/v) Aβ40 (-▼-) and (B) 10% (v/v) of [ΔE22]Aβ42 to 90% (v/v) Aβ42 (-▼-). Binding is expressed as mean fluorescence intensity ± SD. Each figure comprises four independent experiments.

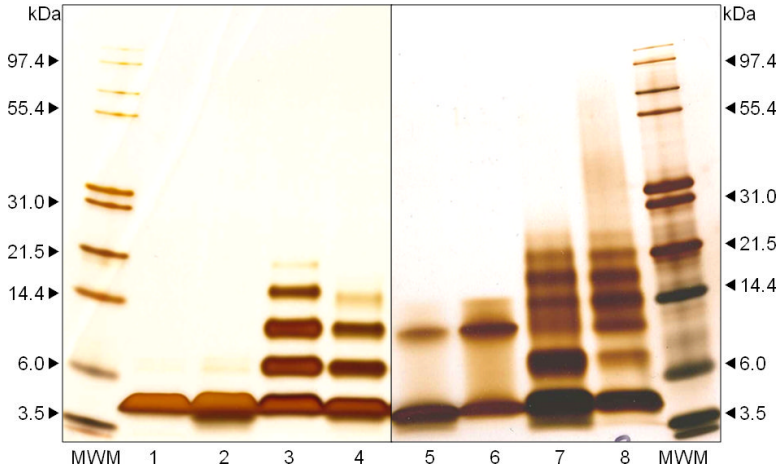

Figure 4.

Oligomerization of Aβ and [ΔE22]Aβ. PICUP, followed by SDS-PAGE and silver staining, was used to study oligomerization of (A) Aβ40, (A) [ΔE22]Aβ40, (B) Aβ42 and (B) [ΔE22]Aβ42. Lane 1, Aβ40 un-cross-linked; Lane 2, un-cross-linked [ΔE22]Aβ40; Lane 3, cross-linked Aβ40; Lane 4, crosslinked [ΔE22]Aβ40; Lane 5, Aβ42 un-cross-linked; Lane 6, un-cross-linked [ΔE22]Aβ42; Lane 7, crosslinked Aβ42; Lane 8, cross-linked [ΔE22]Aβ42. The gels are representative of each of five independent experiments.

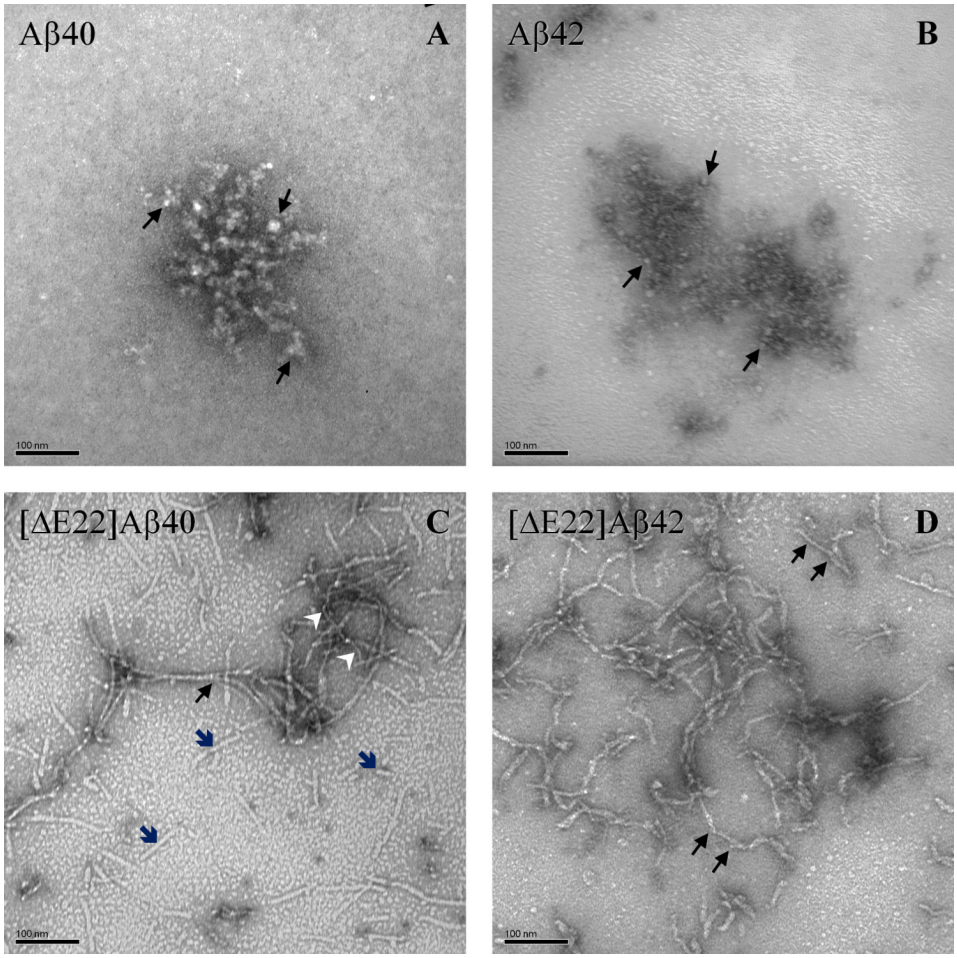

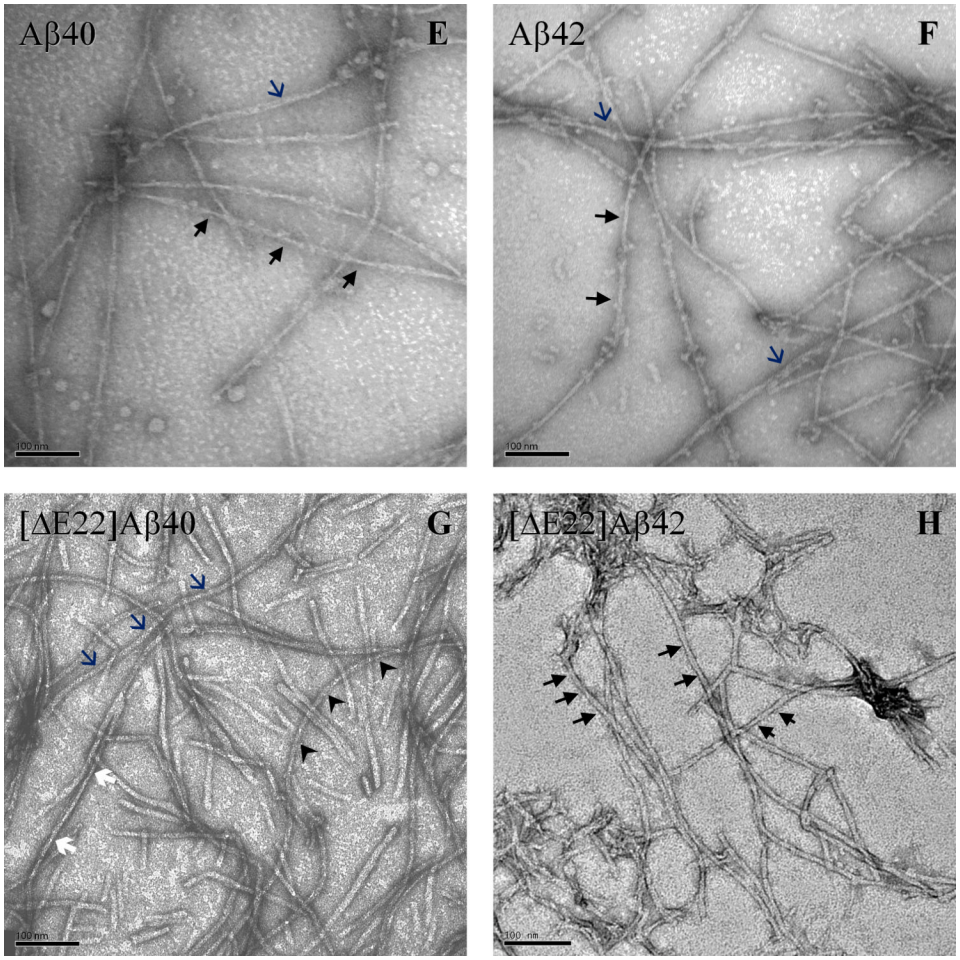

Figure 5.

Morphology of Aβ and [ΔE22]Aβ assemblies. EM was performed on Aβ and [ΔE22]Aβ peptides. A–D show initial assemblies (freshly dissolved samples immediately after sample preparation) of (A) Aβ40, (B) Aβ42, (C) [ΔE22]Aβ40 and (D) [ΔE22]Aβ42 that then were incubated at 37°C in 10 mM phosphate buffer, pH 7.4, for 2-3 weeks. E–H represents fibrillar assemblies of (E) Aβ40, (F) Aβ42, (G) [ΔE22]Aβ40 and (H) [ΔE22]Aβ42 following incubation. The numerous small translucent background structures visible in some samples appear to be non-proteinaceous because they displayed no negative staining. Scale bar indicates 100 nm. The data shown are representative of those obtained in each of three independent experiments.

Table 1

Critical concentration and ΔG^0 of fibril formation.

Peptides	C_r (μM)	p-value	⊗G^0 (kcal/mole)	p-value
Aβ40	1.24 ± 0.09	<0.001	-8.38 ± 0.04	<0.001
[ΔE22]Aβ40	0.58 ± 0.07		-8.85 ± 0.07	
Aβ42	0.87 ± 0.05	<0.001	-8.59 ± 0.03	=0.003
[ΔE22]Aβ42	0.32 ± 0.09		-9.23 ± 0.16	

Aβ40 and [ΔE22]Aβ40, both at concentrations of 20 μM, and Aβ42 and [ΔE22]Aβ42, both at concentrations of 10 μM, were incubated in 10 mM phosphate buffer, pH 7.4, at 37°C for ≈3 weeks. Critical concentration, C_r, is the molar concentration of peptide in the supernate after high-speed centrifugation (436,000 × *g* for 1 h) after cessation of fibril growth. $\Delta G^0 = -RT \ln (1/C_r)$. The values shown are average concentration ± S.D. *p*-values for the significance of the differences between each pair of C_r values or ΔG^0 values are shown to the right of the respective two values. The results comprise four independent experiments.

Table 2

Oligomer frequency distribution.

	Aβ40	[ΔE22]Aβ40	Aβ42	[ΔE22]Aβ42
Monomer	0.28 ± 0.02	0.32 ± 0.03	0.31 ± 0.03	0.34 ± 0.03
Dimer	0.28 ± 0.02	0.30 ± 0.02	0.21 ± 0.04	0.11 ± 0.01
Trimer	0.23 ± 0.01	0.23 ± 0.01	0.11 ± 0.02	0.12 ± 0.02
Tetramer	0.14 ± 0.02	0.13 ± 0.03	0.13 ± 0.02	0.19 ± 0.02
Pentamer	0.07 ± 0.02	0.03 ± 0.01	0.14 ± 0.02	0.15 ± 0.01
Hexamer	ND	ND	0.08 ± 0.03	0.08 ± 0.01
Heptamer	ND	ND	0.02 ± 0.01	0.02 ± 0.01

Aβ and [ΔE22]Aβ peptides were cross-linked using the PICUP method and then monomer and oligomers were visualized by SDS-PAGE and silver staining. The stained gels then were scanned densitometrically and the intensity of each band in a lane was normalized by determining the quotient of band intensity divided by the sum of all band intensities in the lane. The sum of intensities in each lane equal 1 in the absence of rounding errors. The values shown are average ± S.D. The results comprise five independent experiments.